Temperature-Vegetation-soil Moisture-Precipitation Drought Index (TVMPDI); 21-Year Drought Monitoring in Iran using Satellite Imagery within Google Earth Engine

Soroosh Mehravar[a,b], Meisam Amani[c,*], Armin Moghimi[d], Farzaneh Dadrass Javan[a,e], Farhad Samadzadegan[a], Arsalan Ghorbanian[d], Alfred Stein[e], Ali Mohammadzadeh[b,d], S. Mohammad Mirmazloumi[f]

[a] Department of Geomatics, University College of Engineering, University of Tehran, Tehran 1439957131, Iran; (sorooshmehravar, fdadrasjavan, samadz)@ut.ac.ir

[b] Research assistant at LiDAR lab., K. N. Toosi University of Technology, Tehran 1996715433

[c] Wood Environment & Infrastructure Solutions, Ottawa, ON K2E7L5, Canada; meisam.amani@woodplc.com
[d] Faculty of Geodesy and Geomatics Engineering, Department of Remote Sensing and Photogrammetry, K. N. Toosi University of Technology, Tehran 1996715433, Iran; moghimi.armin@gmail.com, a.ghorbanian@email.kntu.ac.ir, a_mohammadzadeh@kntu.ac.ir
[e] Faculty of Geo-Information Science and Earth Observation (ITC), University of Twente, 7522 NB Enschede, the Netherlands; (f.dadrassjavan, a.stein)@utwente.nl
[f] Centre Tecnològic de Telecomunicacions de Catalunya (CTTC/CERCA), 08860 Castelldefels, Spain; sm.mirmazloumi@cttc.es

Corresponding author: Meisam Amani, Email: meisam.amani@woodplc.com

Abstract

Remote Sensing (RS) offers efficient tools for drought monitoring, especially in countries with a lack of reliable and consistent *in-situ* multi-temporal datasets. In this study, a novel RS-based Drought Index (RSDI) named Temperature-Vegetation-soil Moisture-Precipitation Drought Index (TVMPDI) was proposed. To the best of our knowledge, TVMPDI is the first RSDI using four different drought indicators in its formulation. TVMPDI was then validated and compared with six conventional RSDIs including VCI, TCI, VHI, TVDI, MPDI and TVMDI. To this end, precipitation and soil temperature *in-situ* data have been used. Different time scales of meteorological Standardized Precipitation Index (SPI) index have also been used for the validation

of the RSDIs. TVMPDI was highly correlated with the monthly precipitation and soil temperature in-situ data at 0.76 and 0.81 values respectively. The correlation coefficients between the RSDIs and 3-month SPI ranged from 0.07 to 0.28, identifying the TVMPDI as the most suitable index for subsequent analyses. Since the proposed TVMPDI could considerably outperform the other selected RSDIs, all spatiotemporal drought monitoring analyses in Iran were conducted by TVMPDI over the past 21 years. In this study, different products of the Moderate Resolution Imaging Spectrometer (MODIS), Tropical Rainfall Measuring Mission (TRMM), and Global Precipitation Measurement (GPM) datasets containing 15206 images were used on the Google Earth Engine (GEE) cloud computing platform. According to the results, Iran experienced the most severe drought in 2000 with a 0.715 TVMPDI value lasting for almost two years. Conversely, the TVMPDI showed a minimum value equal to 0.6781 in 2019 as the lowest annual drought level. The drought severity and trend in the 31 provinces of Iran have also been mapped. Consequently, various levels of decrease over the 21 years were found for different provinces, while Isfahan and Gilan were the only provinces showing an ascending drought trend (with a 0.004% and 0.002% trendline slope respectively). Khuzestan also faced a worrying drought prevalence that occurred in several years. In summary, this study provides updated information about drought trends in Iran using an advanced and efficient RSDI implemented in the cloud computing GEE platform. These results are beneficial for decision-makers and officials responsible for environmental sustainability, agriculture and the effects of climate change.

Keywords: Drought index; Drought in Iran; MODIS; Monitoring; Remote sensing (RS); TVPMDI

1. Introduction

Drought is a complicated hydrometeorological phenomenon depending on several environmental factors. Drought on land is known as the deficiency in Soil Moisture (SM) being

affected by both Land Surface Temperature (LST) (Ebrahimy et al., 2021) and vegetation conditions (Amani et al., 2017). Degrees of drought has increased over the past decades and are forecasted to be more severe in the future (West et al., 2019). Drought can cause many detrimental results in the environment and economy (Rulinda et al., 2012). Thus, monitoring drought variation (Mahmoudi et al., 2019), over long periods is essential for various applications (Heydari et al., 2018). Accordingly, drought is a common natural disaster that has long been known as one of the human's ecological, hydrological, agricultural and economic concerns (Han et al., 2020; Rulinda et al., 2010).

Drought can be grouped into four categories: (1) meteorological drought defined as a deficit in precipitation; (2) agricultural drought defined as a deficit in SM (Liu et al., 2016); (3) Hydrological drought defined as shortages in run-off, groundwater, or total water storage; and (4) socio-economic drought defined as a shortage in water supply in relation to social demands and response (AghaKouchak et al., 2015). Monitoring of these four drought classes is either performed using *in-situ* meteorological data provided by sparse measurement stations of meteorological and climatological organizations or using Remote Sensing (RS) data. *In-situ* data supply precise measurements of drought-related parameters like rainfall, temperature, and SM, they are collected at a limited number of sites, and thus, do not efficiently support large-scale studies (Xu et al., 2020). Such a limitation may be exacerbated due to possible data gaps and discontinuities, leading to inhomogeneous data (Raziei et al., 2011). Therefore, a suitable alternative solution would be utilizing frequently acquired RS data and spatially consistent data from the Earth’s surface (Dyosi et al., 2021; Hao et al., 2017; Orimoloye et al., 2021c, 2021a; Zambrano et al., 2017).

In addition to several advantages of RS drought monitoring using RSDIs (i.e., synoptic data acquisition, near-real-time observation, consistent data recording) over traditional ground-based

observations, the possibility of employing satellite data with high spatial resolution makes RSDIs more attractive for drought monitoring (AghaKouchak et al., 2015). In fact, the advances in RS technology have led to the acquisition of data in different spatial resolutions, which enhances surface state monitoring. The available high-resolution RS data enables the generation of sophisticated drought indices (i.e., combining different criteria for better representation of drought conditions) at around 1 km and also more satisfactory resolutions of nearly 30 m (Ghaleb et al., 2015). These resolutions are more appealing than other coarse resolution satellite and ground-based drought monitoring procedures, which were conventionally conducted at sub-degree resolutions. Therefore, the diversity of spatial resolution empowers the applicability of RSDIs for global to local drought monitoring studies. Furthermore, previous studies have also acknowledged the use of finer resolution RSDIs for drought monitoring and investigated the effect of spatial resolution on drought event detection(Huffman et al., 2007). For instance, Raziei et al., (2013) reported that coarser spatial resolution drought monitoring resulted in more stable and distinctive drought variability modes in comparison to finer spatial resolutions. Therefore, it is of high importance to consider the suitable spatial resolution of RSDIs based on the study requirements and specifications to achieve the most accurate results. For instance, RSDIs with nearly 1km spatial resolution would be suitable for large-scale studies, while for local studies, especially over agricultural areas in which different types of crops existed, finer resolution RSDIs should be incorporated (Zhou et al., 2020).

Expansion of drought, its severity and environmental effects over a specific period are difficult to be monitored. Therefore, drought is commonly specified by drought indices (Liu et al., 2016). For this purpose, various meteorological indices and RS-based Drought Indices (RSDIs) have been proposed. For instance, the Standardized Precipitation Index (SPI) (McKee et al., 1993; Sharafati

et al., 2020), the Palmer drought severity index (PDSI), the Relative Precipitation Index (RPI), and the Effective Drought Index (EDI) (Byun and Wilhite, 1999) provide location specific information. Alternatively, RSDIs including the Vegetation Condition Index (VCI) (Kogan, 1995), Normalized Difference Vegetation Index (NDVI) (Ding et al., 2011; Rulinda et al., 2011), Temperature Condition Index (TCI) (Kogan, 1995), Vegetation Health Index (VHI) (Kogan, 1995), Temperature–Vegetation Dryness Index (TVDI) (Sandholt et al., 2002), Modified Perpendicular Drought Index (MPDI) (Ghulam et al., 2007), Precipitation Condition Index (PCI) (Du et al., 2013), Temperature-Vegetation-soil Moisture Dryness Index (TVMDI) (Amani et al., 2017), The multivariate standardized drought index (MSDI) (Hao and AghaKouchak, 2014) have been proposed for rapid drought monitoring over large areas. Table 1 depicts the most popular RSDIs and their formulas in which different types of drought indicators have been used.

Table 1. Popular RSDIs and their formulas.

Index	Formula	Parameter	Reference
VCI	$\frac{NDVI_{i,t}-NDVI_{i,min}}{NDVI_{i,max}-NDVI_{i,min}}$ (1)	$NDVI_{i,t}$ refers to the NDVI value for the pixel i at the time of t, $NDVI_{i,min}$ and $NDVI_{i,max}$ denotes the minimum and maximum NDVI values in the long time series respectively, for pixel i	(Kogan, 1995)

TCI	$\frac{LST_{i,max}-LST_{i,t}}{LST_{i,max}-LST_{i,min}}$ (2)	$LST_{i,t}$ is the LST value for pixel i at the time of t, $LST_{i,min}$ and $LST_{i,max}$ refer to the minimum and maximum LST values in the long time series, respectively, for pixel i	(Kogan, 1995)
VHI	$\alpha VCI + (1-\alpha)TCI$ (3)	α and $(1-\alpha)$ are the weights of the VCI and TCI, respectively. α was set at 0.5 in this paper.	(Kogan, 1995)
TVDI	$\frac{T_{NDVI_i}-T_{NDVI_{i,min}}}{T_{NDVI_{i,max}}-T_{NDVI_{i,min}}}$ (4)	T_{NDVI_i} represent the LST in the NDVI-LST triangle space at a pixel, $T_{NDVI_{i,min}}$ and $T_{NDVI_{i,max}}$ refer to minimum and maximum surface temperature in the NDVI-LST triangle space respectively, for pixel i, which calculated as follow: $T_{NDVI_{i,min}} = a + bNDVI_i$ (5) $T_{NDVI_{i,max}} = a' + b'NDVI_i$ (6) a, b, a', and b' are the undetermined coefficients, related to the dry edge in the triangle. The parameters a and b were set equal to their average values used by (Schirmbeck et al., 2018).	(Sandholt et al., 2002)
MPDI	$\frac{\rho_{red} + M_{\rho_{NIR}} - f_v(\rho_{v,red} + M_{\rho_{v,NIR}})}{(1-f_v)\sqrt{M^2+1}}$ (7)	$\rho_{v,red}$ and $\rho_{v,NIR}$ refer to green and healthy vegetation reflectance values of the red and NIR bands, respectively, f_v is the fraction of vegetation cover, M implies the slope of the soil line equation. M was set at 1.163 (Amani et al., 2017). The f_v parameter is calculated using the formula presented by (Ghulam et al., 2007).	(Ghulam et al., 2007)
MSDI	$MSDI = \varphi^{-1}(p)$ **(8)**	MSDI is based on the states of precipitation and SM. It probabilistically combines the SPI and the Standardized Soil Moisture Index (SSI) for drought characterization. φ is the standard normal distribution function. Equation (8) transforms the joint probability to the MSDI that is in the same space as the original SPI and allows cross-comparison of different drought indices, such as SSI.	(Hao and AghaKouchak, 2014)
NDWI	$\frac{\rho_{NIR}-\rho_{SWIR}}{\rho_{NIR}+\rho_{SWIR}}$ **(9)**	The Normalized Difference Water Index (NDWI) is one of the most popular RSDIs. It is sensitive to changes in liquid water content of vegetation. ρ_{NIR} and ρ_{SWIR} are reflectance values of near-infrared and short-wave infrared.	(Gao, 1996)

Table 1. (continued).

Index	**Formula**	**Parameter**	**Reference**

MIDI	$\alpha \times PCI + \beta \times SMCI + (1 - \alpha - \beta) \times TCI$ **(10)** $PCI = \frac{P_i - P_{min}}{P_{max} - P_{min}}$ **(11)** $SMCI = \frac{SM_i - SM_{min}}{SM_{max} - SM_{min}}$ **(12)**	The Microwave Integrated Drought Index (MIDI) estimates short-term drought, particularly the meteorological drought over semi-arid regions. It integrates precipitation (P), SM, and LST. Each variable is linearly scaled from 0 to 1 for each pixel based on absolute minimum and maximum values over time to monitor drought relatively. In Equation (10), TCI, PCI, and SM Condition Index (SMCI) are RSDIs. α and β also present the weight of single index while constituting the integrated drought indices.	(Zhang and Jia, 2013)
OMDI/ OVDI	OMDI: Constrained Optimization for TCI, PCI, and SMCI OVDI: Constrained Optimization for VCI, TCI, PCI, and SMCI	The optimized versions of meteorological drought index (MDI) and the vegetation drought index (VDI) were proposed using multi-source satellite data, including precipitation, temperature, SM and vegetation information. The Constrained Optimization method was adopted to determine the optimal weights of VCI, TCI, PCI, SMCI indices generating combined drought indices. TRMM stands for Tropical Rainfall Measuring Mission.	(Hao et al., 2015)
ESI	$f_{RET} = \frac{ET}{ET_{ref}}$ **(13)**	The Evaporative Stress Index (ESI) is an indicator of agricultural drought regarding the timing and magnitude of peak correlations with spatially distributed yield observations. It defines fluctuations in the actual/reference evapotranspiration (ET) ratio, retrieved using remotely sensed inputs of LST and Leaf Area Index (LAI). The ESI presents standardized anomalies in a normalized clear-sky ET ratio (f_{RET}), in which ET is actual ET and ET_{ref} is a reference ET scaling flux used to minimize impacts of non-moisture related drivers on ET (e.g., seasonal variations in radiation load).	(Anderson et al., 2015)
OSDCI	$\alpha \times P + \beta \times LST + \gamma \times NDVI$ **(14)**	Optimal Scaled Drought Condition Index (OSDCI) is a developed version of SDCI, an agricultural drought index derived from multiple RS datasets including precipitation (P), LST, and vegetation index (NDVI). It was proposed since SDCI is not applicable to certain areas. OSDCI can address uncertainties associated with the coarse resolution of precipitation input, the fixed lag time between precipitation deficit and vegetation responses, experimental weights (α, β and γ), and an arbitrary classification scheme. It should be noted that the weights for OSDCI are decided by the constrained optimization method.	(Guo et al., 2019)

Studying drought over large-scale areas requires the processing of a massive amount of data and, thus, poses the critical limitation of high computational complexity. Despite the significant advances in RS and its capability to provide drought data as a time-series over large areas, a considerable challenge regarding big data processing remains (Adedeji et al., 2020; Ghorbanian et al., 2020). In recent years, cloud-computing platforms, including Google Earth Engine (GEE),

have efficiently tackled this limitation. GEE is a high-performance cloud-computing platform supporting big geospatial data processing and analyzing at local to global scales (Amani et al., 2020a; Gorelick et al., 2017). GEE contains a consolidated resource of open-access RS datasets, along with a variety of algorithms to extract information for Earth's surface monitoring (Amani et al., 2020b, 2017). These advantages have contributed to GEE's applicability for large-scale drought monitoring (Aksoy et al., 2019; Córdova et al., 2020; Khan et al., 2020; Okal et al., 2020; Sazib et al., 2018). Aksoy, Gorucu, and Sertel 2019 studied drought severity in Turkey using MODIS imagery to determine various drought indices. Khan et al. 2020 employed different data sources to investigate the emergence of drought in the Potohar plateau. Other drought studies using RS data have modeled the spatio-temporal statistical behavior of RSDIs (Oesting and Stein, 2018) and the movement of drought (Rulinda et al., 2013).

Iran is one of the driest countries worldwide and several studies have explored drought conditions and intensity using *in-situ* and RS data. However, most of these studies were over relatively small areas (e.g., one province) and short periods (e.g., a few years) (see (Bajgiran et al., 2008; ShadA et al., 2017; Sobhani et al., 2019) as examples). There are only a few studies in the literature focusing on drought monitoring of entire Iran mostly over a few years using relatively traditional methods. For example, Zarch et al. 2011, used the SPI and RDI meteorological drought indices (i.e., derived from 40 meteorological synoptic stations) for mapping drought severity in Iran during 1 year (1999–2000). Shahabfar, Ghulam, and Eitzinger 2012 assessed the performance of two RSDIs, including PDI and MPDI, derived from MODIS images. Zarei, Sarajian, and Bazgeer 2013 employed the SPI meteorological-based index and multiple RSDIs (i.e., NDVI, VCI, VHI, and TCI), derived from AVHRR images, for drought monitoring. Emadodin, Reinsch, and Taube 2019 employed the PVI and De Martonne aridity index (I_{DM}) for long-term drought

monitoring (1950-2017) in different climate zones in Iran. Finally, Hosseini et al. 2020 studied the variations of drought characteristics using the data of the Global Precipitation Climatology Center-Drought Index (GPCC-DI).

The main objective of this study is drought monitoring in Iran over the past two decades by using the most accurate RSDI in the GEE platform. Considering the previous studies discussed above, the main contributions and novelties of this study are: (1) The proposed TVMPDI that is a composite of vegetation, LST, SM, and precipitation drought indicators; (2) Validation and comparison of RSDIs for drought monitoring in Iran using the high amount of *in-situ* data (collected from 228 meteorological stations); (3) Local and global drought monitoring in Iran over 21 years using the most accurate RSDI; (4) GEE is employed for this purpose for the first time.

2. Data and Methodology

2.1. Study area

Iran is located in the northeastern part of Asia between latitudes and longitudes of 24° - 40° N and 44° - 64° E, respectively, and covers a total area of approximately 1.6 million km^2. Different land cover types exist in the study area, varying from dense forest regions to uncovered plains (Ghorbanian et al., 2020). As can be seen in Fig. 1(a) and (b), the northern part of the country includes the Caspian Sea and dense forest covers, mostly located at Alborz Mountains. The Zagros Mountains are situated in the west, spanning from the north to the south of Iran, and include different types of vegetative land covers. The presence of these high mountains reduces the entry of rain clouds into the central and southeastern parts of the country, and thus, these regions are mostly covered by uncovered plains and sand deserts (e.g., the Lut and Kavir deserts). Finally, the southern border of Iran is formed by the long coastlines of the Persian Gulf and the Oman Sea. Although the majority of Iran is dry, the country has diverse climate conditions due to covering

massive latitudinal ranges and geographical characteristics (Alizadeh-Choobari and Najafi, 2018). Moreover, the topographic and climatic conditions cause a significant precipitation variation across the country, ranging from 100 mm/year to 1100 mm/year from southeastern to northern parts (Darand and Daneshvar, 2014). In recent decades, Iran has been adversely affected by the increase in meteorological droughts, which has led to the land degradation process (Emadodin et al., 2019). The meteorological drought is the principal driving force of land degradation, which occur due to the extended period of precipitation deficiency.

2.2. Datasets

2.2.1. RS data

Three products of the MODIS satellite, TRMM and GPM images were used for the implementations of drought in GEE. Table 2 shows more information about these products.

Table 2. Information about GEE products used in this study.

Name of product (ID of image collection)	Spatial resolution	RSDIs generated from the product	Bands used in drought indices	Number of images
Terra Surface Reflectance-Daily Global (MODIS/006/MOD09GQ)	250m	MPDI, TVMDI, TVMPDI	Red and NIR	7246
Terra Land Surface Temperature and Emissivity-Daily Global (MODIS/006/MOD11A1)	1km	TVDI, TVMDI, TCI, VHI, TVMPDI	Daytime and nighttime LST	7247
Terra Vegetation Indices 16-Day Global (MODIS/006/MOD13Q1)	250m	TVDI, VCI, VHI, MPDI	NDVI	460
TRMM 3B43: Monthly Precipitation Estimates (TRMM/3B43V7)	0.25 degrees	TVMPDI	Precipitation	237
Monthly Global Precipitation Measurement (GPM) v6 (NASA/GPM_L3/IMERG_MONTHLY_V06)	0.1 degrees	TVMPDI	Precipitation	16

2.2.2. Meteorological data

The total monthly precipitation data collected at the 228 meteorological stations of the Islamic Republic of Iran Meteorological Organization (https://www.data.irimo.ir/) were used in this study to validate and compare the results of RSDIs. Fig. 1(c) demonstrates the spatial distribution of these stations. It should be noted that the location of each station is assumed to correspond to a single image pixel with 250m size in the produced drought maps.

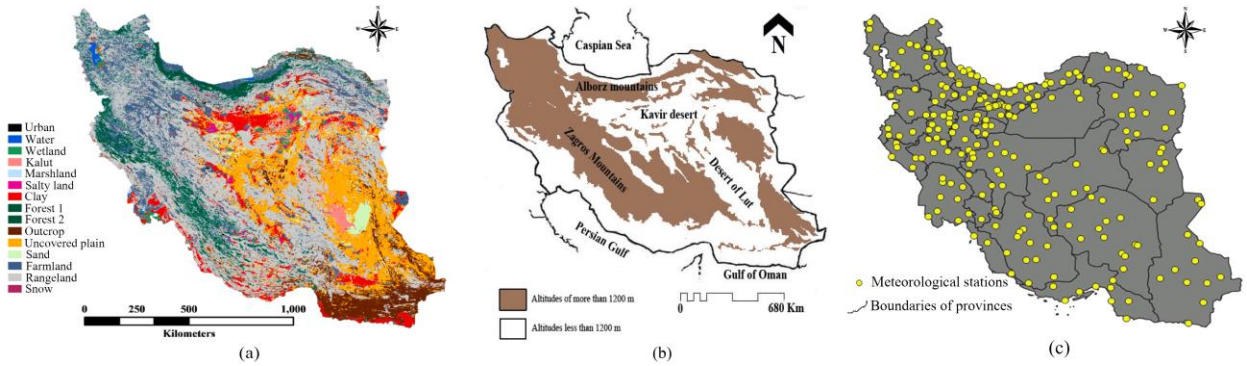

Figure 1. (a) land cover map of Iran (b) Two main deserts and two mountainous chains in Iran (Sanei and Zakaria, 2011) (c) distribution of 228 meteorological stations.

2.3. Proposed TVMPDI index

In a recent study, Amani et al. (2017) proposed the TVMDI to characterize the drought variations, in which vegetation, LST and SM have been taken into account. On one side, many other novel indices have incorporated precipitation data into the RSDIs to develop more accurate indices (Hao et al., 2015). In this study, TVMDI is integrated with the precipitation component to form the Temperature-Vegetation-soil Moisture-Precipitation Drought Index (TVMPDI).

The TVMDI formula which is comprised of LST, SM and Perpendicular Vegetation Index (PVI) parameters is calculated in (15), and the computation of PVI and SM is given in (16) and (17):

$$TVMDI = \sqrt{\mathrm{LST}^2 + \mathrm{SM}^2 + \left(\frac{\sqrt{3}}{3} - \mathrm{PVI}\right)^2} \qquad (15)$$

$$\mathrm{PVI} = \frac{\rho_{\mathrm{NIR}} + \mathrm{M}\rho_{\mathrm{red}} - \mathrm{I}}{\sqrt{\mathrm{M}^2 + 1}} \quad (16)$$

$$\mathrm{SM} = \frac{\rho_{\mathrm{NIR}} + \frac{\rho_{\mathrm{red}}}{\mathrm{M}} - \mathrm{b}}{\sqrt{\frac{1}{\mathrm{M}^2} + 1}} \quad (17)$$

where ρ_{red} and ρ_{NIR} in SM and PVI specify the atmospherically corrected reflectance values of the red and NIR bands, respectively; M and I are slope and interception of the soil line equation respectively. In accordance with (Amani et al., 2017), the values of the M and I parameters used in this study were set at 1.163 and 0.017 respectively. b refers to the interception of the perpendicular line with the soil line (Amani et al., 2016). The proposed TVMPDI formula in which the LST, SM, PVI and precipitation components are involved is defined in:

$$\mathrm{TVMPDI} = \frac{1}{2}\sqrt{\mathrm{LST}^2 + \mathrm{SM}^2 + (1 - \mathrm{PVI})^2 + \mathrm{P}^2} \quad (18)$$

Where P refers to the TRMM/ GPM that are selected as the precipitation component due to their free availability, global coverage and near real-time data. In this study, the values for each component of (18) were normalized between 0 and 1 using the eq. (19):

$$\mathrm{Normallized\ V_i} = \frac{\mathrm{V_i} - \min(\mathrm{V})}{\max(\mathrm{V}) - \min(\mathrm{V})} \quad (19)$$

where V is one of the four variables of PVI, SM, LST, or P and $\mathrm{V_i}$ is the $\mathrm{i^{th}}$ data in V = ($\mathrm{V_1}, \mathrm{V_2}, \ldots, \mathrm{V_i}$). This step is done to make the LST, PVI, SM, and precipitation comparable with one another, hence conversion of the final TVMPDI dryness values between 0 and 1. The maximum and minimum values of each component in (19) are obtained over the desired time span and study area. The general description of TRMM and GPM precipitation data used in TVMPDI is explained in subsection 2.3.1 and 2.3.2 respectively.

2.3.1. The Tropical Rainfall Measuring Mission (TRMM) precipitation

The TRMM satellite is a NASA–JAXA corporation, launched in November 1997 to estimate tropical rainfall and currently operates between 50 ° North and 50° South with a 3-hour temporal resolution and a 0.25° spatial resolution (Zhang and Jia, 2013). The precipitation data can derive from different sensors of TRMM satellites like the precipitation radar (PR), the TRMM microwave imager (TMI), and the visible and infrared radiometer system (VIRS) (Labarrere et al., 2011; Zhang and Jia, 2013).

2.3.2. Global Precipitation Measurement (GPM)

The GPM mission is a joint project between JAXA and NASA to provide timely and accurate global precipitation observation from Integrated multi-satellite retrievals for GPM (IMERG) (Skofronick-Jackson et al., 2017). Such measurements help forecast life-threatening events and improve the understanding of the water and energy cycle. GPM is more advanced than TRMM because it is equipped with extra channels on both the dual-frequency precipitation radar (DPR) and the GPM Microwave Imager (GMI) (i.e., it is able to detect light rain and snowfall) (Hou et al. 2008, 2014). GPM has also developed TRMM's reach in terms of global coverage, intercalibrate, merge, and interpolate precipitation datasets with other microwave radiometers, delivery of data items with less delay, and simplified data availability (Skofronick-Jackson et al., 2017).

2.4. Methodology

The first objective of the study was comparing the accuracy and efficiency of several RSDIs to find the most suitable drought index for Iran. To this end, the meteorological precipitation and soil temperature data were used to validate the results of RSDIs, calculated for the period of 2000-

2020. The superior RSDI was subsequently used to monitor different aspects of drought across the country. The spatial and temporal variations of drought, distribution of drought trends, drought severity classification maps and drought variations for all provinces were also investigated. The step-by-step workflow of this study is illustrated in Fig. 2.

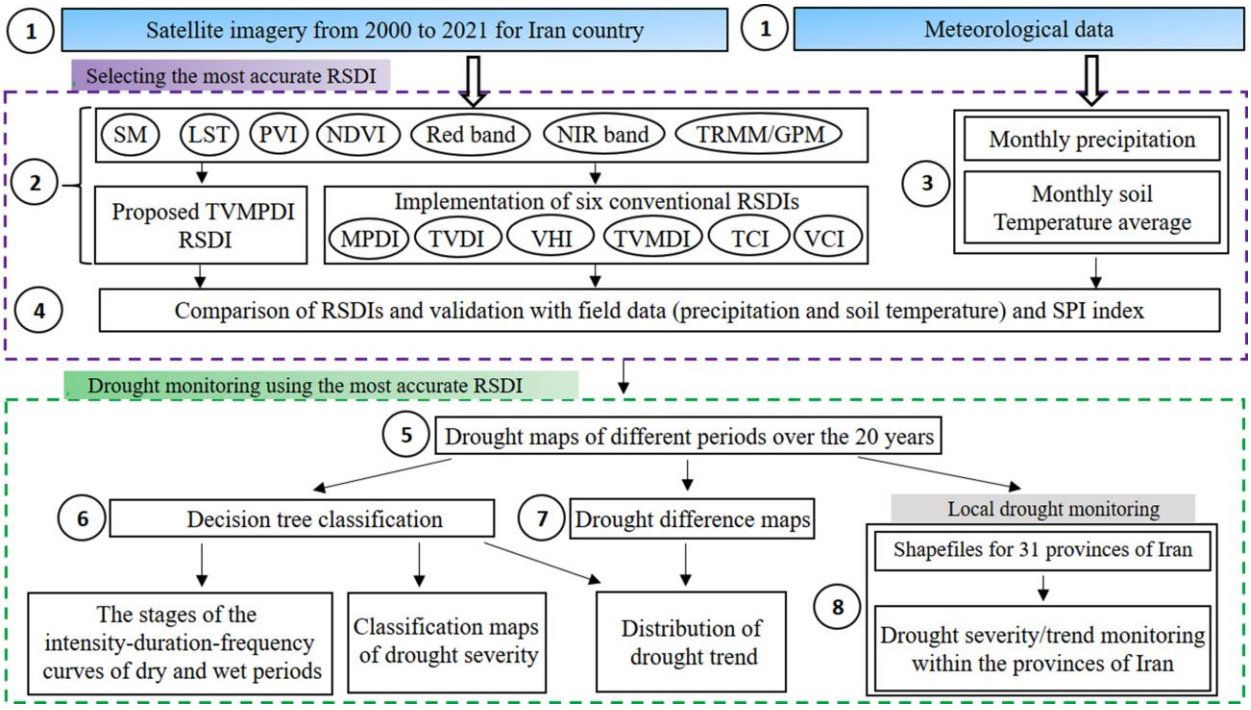

Figure 2. The proposed methodology flowchart for drought monitoring in Iran using GEE.

(1) Data Preparation: Different products of MODIS, TRMM and GPM were used to compute RSDIs. In this study, RS data from 20th March 2000 to 20th March 2021 have been analyzed for drought monitoring. The meteorological data including monthly precipitation and soil temperature average was also used to validate and compare the performance of RSDIs.

(2) RS Drought monitoring methods: In this study, the VCI, TCI, VHI, TVDI, MPDI, TVMDI, as some of the most popular RSDIs (Amani et al., 2017; Huang et al., 2020; Wang et al., 2018; Zhang et al., 2016) were employed to be compared with the proposed TVMPDI. The comparisons are accomplished using the *in-situ* data of Irans'

meteorological stations over 21 years. The configurations of constant parameters involved in these RSDIs are provided in Table 1 as well.

(3) Meteorological index calculation: Using the precipitation data, the SPI index was computed as a criterion for validation of RSDIs. 1-month, 3-month, and 6-month and 12-month timescales were set for the SPI index. All SPI calculations in this study were performed using the SPI code provided by Farahmand and AghaKouchak, (2015).

(4) Comparison of RSDIs and validation with meteorological data: The correlation between the monthly results of RSDIs (from 2000 to 2020) calculated for all 228 stations with the corresponding monthly *in-situ* data records has been computed. In fact, 252 values for each RSDI were calculated for each meteorological station to be compared with the corresponding 252 *in-situ* measurements. This procedure has been done using both types of selected *in-situ* data. SPI is also a well-known meteorological drought index used in frequent drought studies (SafarianZengir et al., 2020). Therefore, the SPI index has been selected for the validation step due to its popularity and efficiency reported in the literature. Using the SPI, which employs *in-situ* rainfall data, the drought severity mapping at the meteorological stations over any desired period can be obtained (Amirataee and Montaseri, 2017; SafarianZengir et al., 2020; Sobhani et al., 2020). Since there are lag effects for vegetation responses to meteorological drought, most studies (e.g., (Huang et al., 2020; Wang et al., 2014)) take the lag effect into account by comparing the RSDIs with timescale SPIs (especially three-month SPI) (Zambrano et al., 2016; Zormand et al., 2017). In this study, the correlation coefficients (r) between the monthly variations of RSDIs and 1-month, 3-month, 6-month and 12-month scales of SPI were calculated. The r results were used to show the assessment accuracy of the RSDIs. The seasonal results of the selected

RSDIs were also calculated to compare the long-term variation pattern of each RSDI. To this end, the average value of every 3-month drought map was computed by all RSDIs within the whole boundary of Iran.

(5) Drought maps at different time scales: Aiming at drought monitoring over the 21 years using the most accurate RSDI, numerous drought maps were generated for monthly, 3-month, 6-month and yearly intervals. In this study, the starting date of the 21 years was set on 20th March 2000 when is the first day of spring in Iran local time. Therefore, April, May and June are the months that approximately represent the local time of the spring season.

(6) Decision tree classification: The decision tree classification was implemented on every drought map at each time scale to create the intensity-duration-frequency curves of dry and wet periods, and classified severity/trend maps. For example, every 6-month drought map was classified, then the number of pixels belonging to each drought class was calculated to form the intensity-duration-frequency curves of dry and wet periods.

(7) Drought difference maps: Using the drought difference maps along with the decision tree classification, the distribution of drought trends was mapped for various periods. The difference maps were obtained by subtracting the yearly computed drought maps from one another.

(8) Local drought monitoring within 31 provinces of Iran: Since the spatial distribution of drought trends is considerably heterogeneous, the drought changes within the 31 provinces of Iran were monitored. This local monitoring was done using the georeferenced shapefiles of the provinces and the initially generated drought maps from step (1).

3. Results

3.1.Comparison of RSDIs

The drought maps produced from all selected RSDIs were initially produced for different time scales (monthly, seasonal, half-yearly, and yearly). To this end, the mean values of the dryness indicators (i.e., vegetation, LST or SM) over the desired time scales have been employed. In the case of the NDVI index, the maximum value composite method was used to synthesize the monthly NDVI and to reduce the effect of the atmosphere. All RSDI values were normalized between 0 and 1 to make the results comparable.

The scatter plot of monthly RSDIs values and monthly average of *in-situ* precipitation in Tehran (Mehrabard), Tabriz, Ahvaz, Mashhad, and Sari stations located in different climatic regions is shown in fig. 3. In fig. 3, each scatter plot contains 252 points representing the monthly values of RSDIs and in-situ precipitation over the 21 years. The scatter plot of monthly RSDIs values and monthly average of *in-situ* soil temperature data is illustrated in fig.4. These monthly comparisons were done for all 228 stations and the average results of *r* values were shown in Table 3. The remotely sensed precipitation on the vertical axis in fig. 3 and 4 represent the TRMM and GPM values.

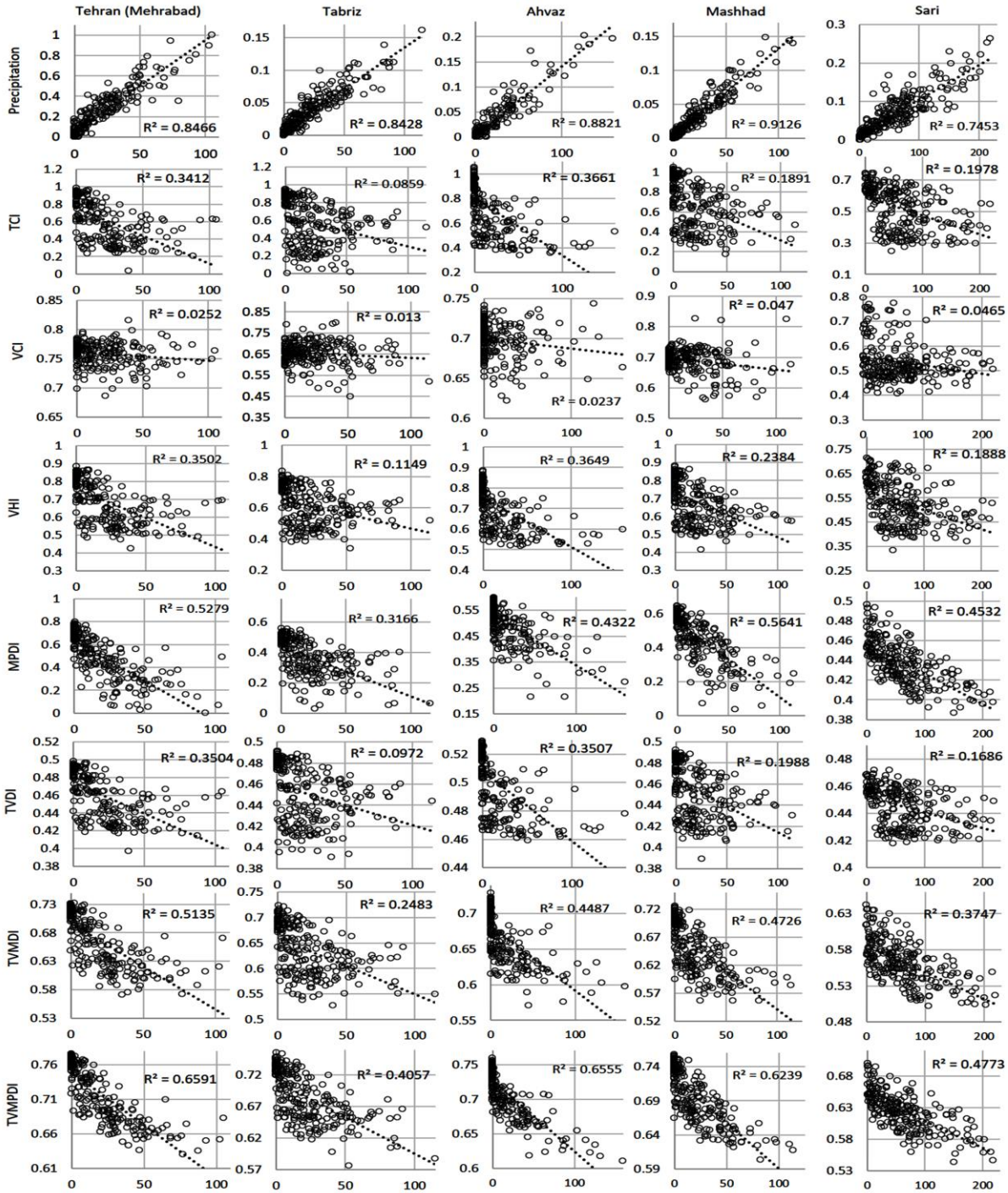

Figure 3. The scatter plot of monthly RSDIs results and monthly meteorological precipitation data over 21 years in 5 stations located in different climatic regions. The unit of meteorological precipitation data is mm/month (Horizontal axis)**.**

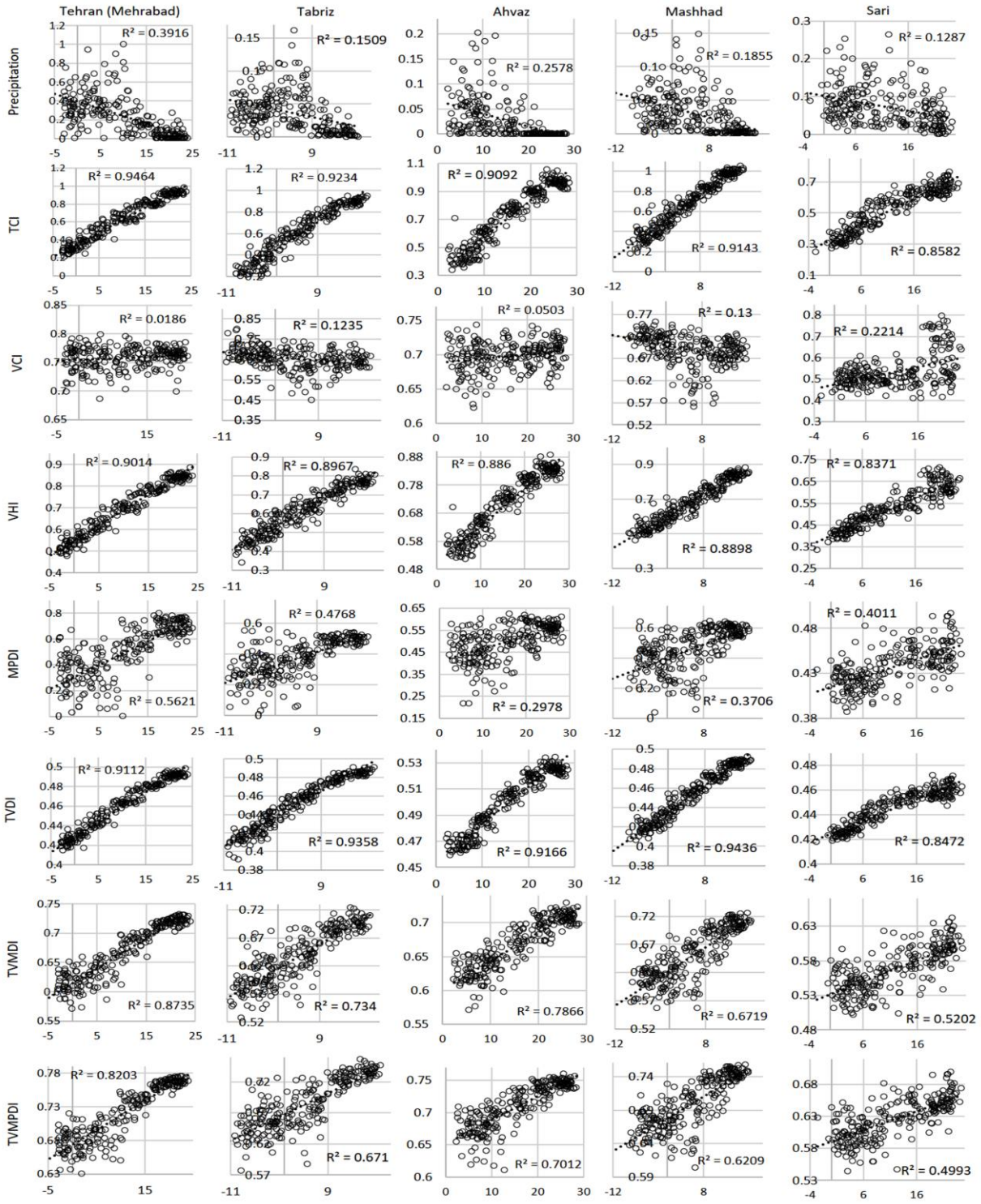

Figure 4. The scatter plot of monthly RSDIs results and monthly average of meteorological soil temperature data over 21 years in 5 stations located in different climatic regions. The unit of the meteorological soil temperature data is degree Celsius (Horizontal axis)**.**

After producing the monthly drought maps using all RSDIs over the 21 years, the results were compared with the results of different SPI time-scales. The input of all SPI time-scales were the monthly in-situ precipitation data of the stations over 21 years. After the computation of the correlations between the RSDIs and SPI time-scales in each station, the average of *r* values at SPI time-scale was calculated. The average values of *r* between the monthly results of RSDIs and 1-month, 3-month and 6-month scales of the SPI were provided in Table 3. It is worth mentioning that the negative correlations between the SPI and TVDI/MPDI were multiplied by –1 in the results to emphasize the correlation strength rather than its direction.

Table 3. Validation results of RSDIs. The correlation coefficients were calculated based on time series from March 2000 to February 2021. SPI1, SPI3, SPI6 and SPI12 refer to 1-month, 3-month, 6-month and 12-month scales of the SPI. Correlation coefficients are significant at p = 0.05. The largest correlations are in bold letters.

drought index	MPDI	TCI	VCI	TVMDI	VHI	TVDI	TVMPDI
Monthly precipitation	0.65	0.48	0.2	0.66	0.46	0.49	**0.76**
Monthly soil temperature average	0.64	**0.95**	0.33	0.84	0.92	0.94	0.81
SPI1	0.23	0.12	0.04	0.25	0.1	0.18	**0.27**
SPI3	0.25	0.13	0.07	0.27	0.12	0.2	**0.28**
SPI6	0.22	0.1	0.05	0.24	0.09	0.17	**0.26**
SPI12	0.2	0.08	0.03	0.21	0.07	0.15	**0.24**

According to Table 3, RSDIs indicated greater *r* with *in-situ* data when they were compared with 3-month SPI. On the contrary, the lowest overall *r* was observed for the monthly SPI. The average *r* of all stations, indicating the overall performance of each RSDI showed that TVMPDI outperformed all other indices for the different SPI time-scales. TVMPDI was highly correlated with the monthly precipitation and soil temperature in-situ data at 0.76 and 0.81 values respectively. However, TCI could outperform the other RSDIs when compared by monthly soil

temperature average. On the other hand, the VCI and VHI showed the weakest performances, respectively.

The seasonal drought changes in Iran using the RSDIs during 2000-2020 were also calculated and shown in Fig. 5. The seasonal results were made out of averaging mean dryness values of every season's months. These charts help in understanding the overall drought trend in each season. Based on the drought trendlines and charts of the majority of indices illustrated in Fig. 5, spring, summer, and autumn seasons were undergone an overall descending change over the 21 years, while winter showed a mild growth. Considering the TVMPDI, the least dryness level in spring, summer, autumn and winter occurred in 2000, 2000, and 2010, and 2020 respectively. The precipitation rate using TRMM and GPM data indicated an incremental trend in Spring and Summer, while Autumn and Winter have faced a long-term declining trend of rainfall.

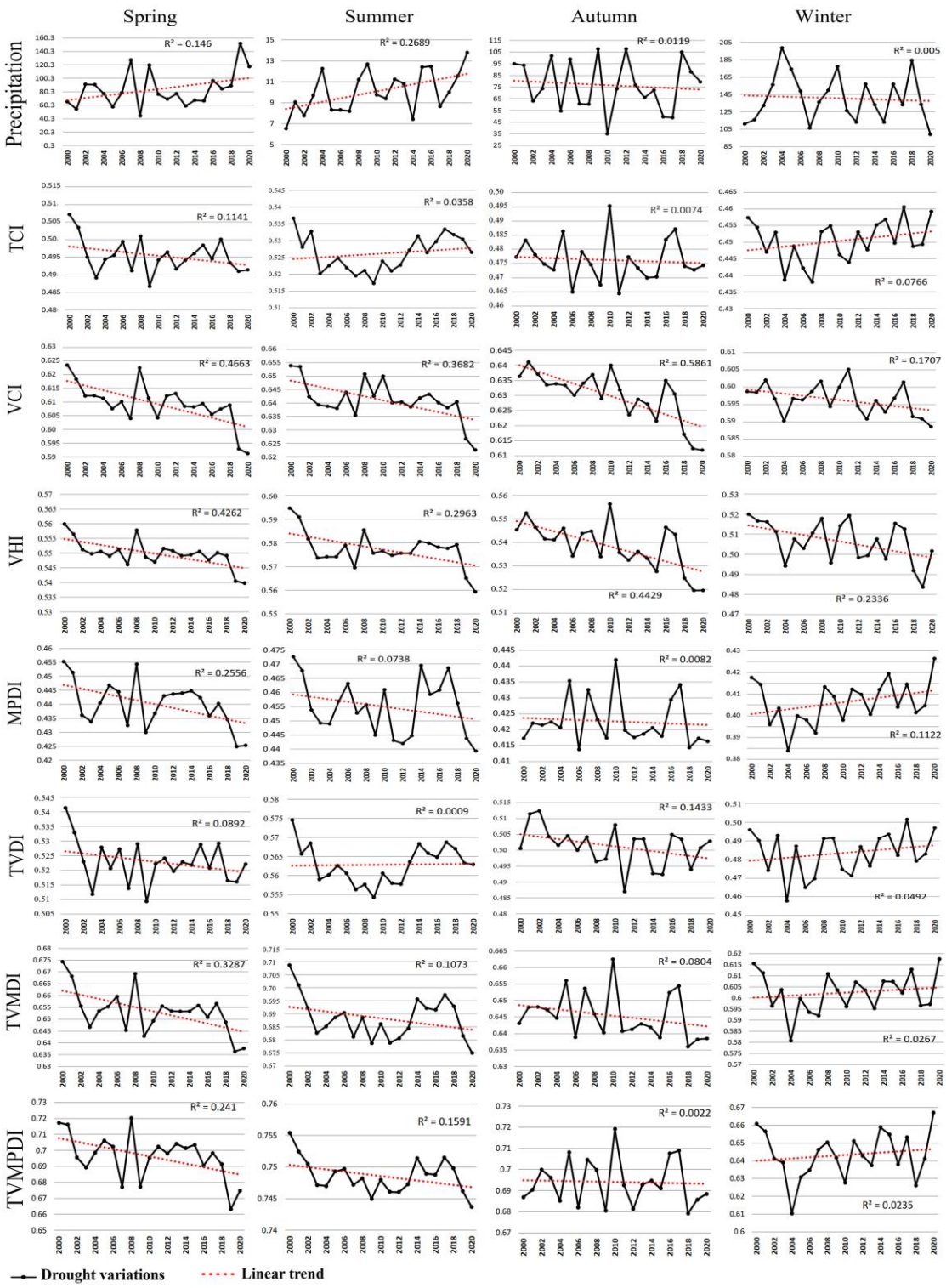

Figure 5. Drought Characteristics of Iran based on the seasonal basis during 2000–2020. Precipitation refers to TRMM/GPM data in mm.

3.2. Drought monitoring using the RS index

4.2.1 Intensity, duration, and frequency of dry and wet periods

The drought intensity, duration, and frequency charts of Iran using the TVMPDI between 2000 and 2020 are illustrated in Fig. 6. Displaying the frequency variations of pixels with specific ranges of the TVMPDI can help to find the meaningful trends of drought over the desired period. Fig. 6 is produced for 6-month scales due to the noticeable difference in the amount of precipitation between the first and second half of the year in Iran. As depicted in Fig. 6(a), the highest percentage of areas with extremely severe drought (red bar chart) belongs to the years 2000, 2001 and 2002, respectively. The area affected by extremely severe drought has significantly decreased for the next 17 years. What stands out from the charts is that Iran experienced its greatest wet periods (TVMPDI = 0.50 or less) in the second half of 2004, 2018 and 2019, respectively. The driest half-year during the 21 years occurred in the first half of 2000 and 2008, respectively. Since the spatial resolution of TVMPDI drought maps is 250m, the area of regions belonging to each drought class can be calculated by multiplying the number of pixels in each drought class by 0.0625 km^2. By comparing the driest (2000) and wettest year (2019), it can be inferred that at least 187500 km^2 (3 million pixels) of Iran's dry area turned into wet regions. The variation of the 6-month TVMPDI average, max and min values calculated for the entire country is demonstrated in Fig. 6(b). The equation of the best-fit linear trendline demonstrated a descending drought trend over the 21 years (slope = -0.0002). The most intensive and least drought levels occurred in 2000 and 2019 when the yearly mean TVMPDI were 0.715 and 0.6781, respectively. The noticeable difference between the drought map pixels having the min and max TVMPDI values in each half-year (Fig. 6(b)) indicates that a wide range of dryness level can be found in different parts of Iran.

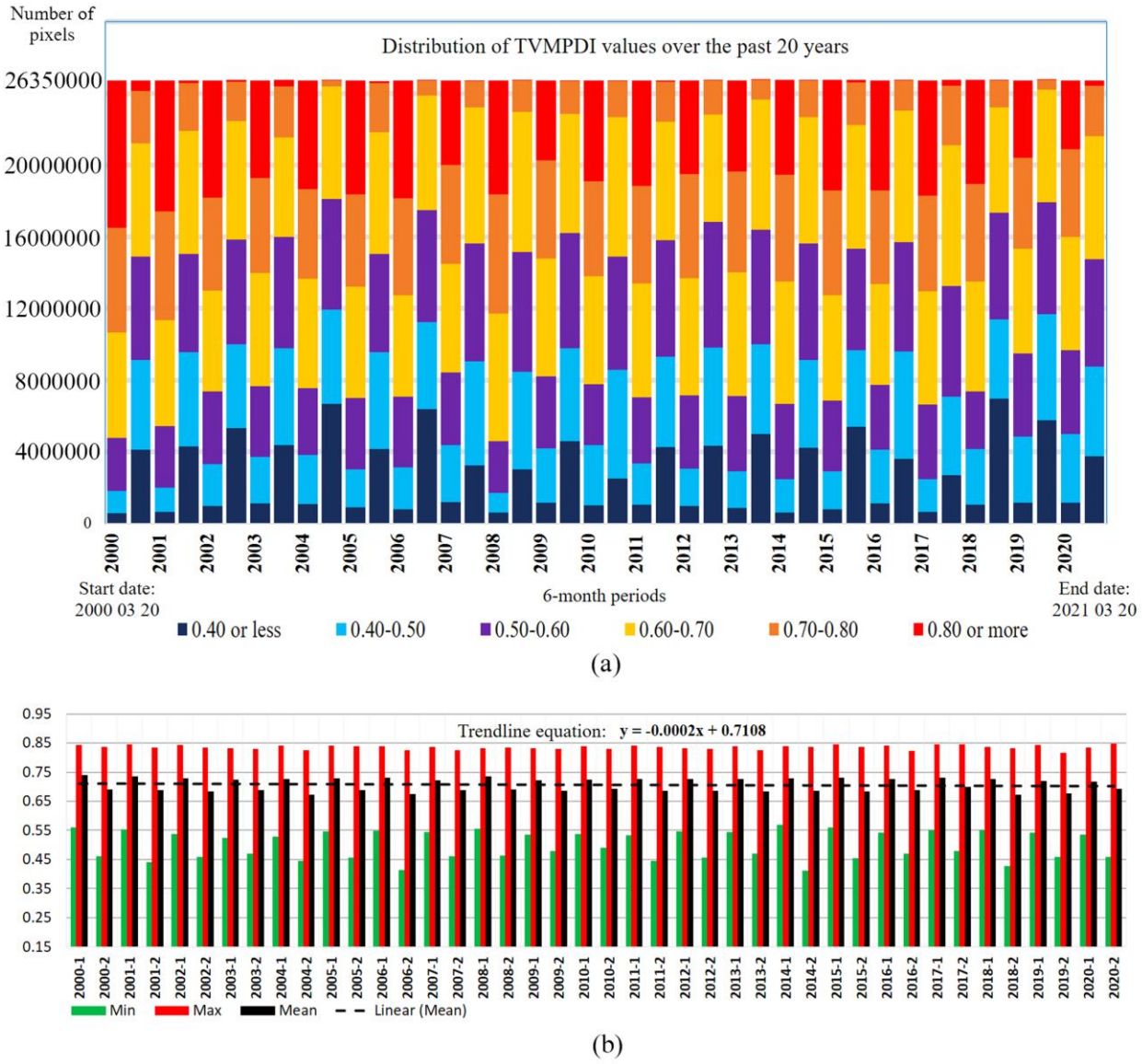

Figure 6. (a) The intensity-duration-frequency curves of dry and wet periods in Iran using the TVMPDI (b) Mean, Max and Min variations of TVMPDI across Iran.

4.2.2 Distribution of drought trend

To evaluate the spatio-temporal distribution of drought changes, the classification of three difference maps has been shown in Fig. 7. Since drought is commonly known as the long-term changes of dryness values, the difference maps indicating the increase or decrease of drought were derived by comparing three annual TVMPDI maps. These three maps were computed for 2000,

2010, and 2020 to cover the decadal and twenty-year drought changes. Based on the maps and statistics provided in Fig. 7, the drought trend over the first decade of the past 21 years was noticeably different from the second decade. Fig. 7(a), (b) show that a considerable portion of regions in Iran (37%) experienced different levels of increment in the TVMPDI values from 2000 to 2010. The corresponding regions were mostly scattered in the middle and northernmost parts of Iran. Fig. 7(c) also represents the severe drought exacerbation over the second decade (more than 0.02 increase in the TVMPDI values). This trend was observed in a marginal strip in the southwest of Iran, while the northwestern and northeastern regions faced different ranges of decrease in dryness levels.

The general drought trend over the last decade (from 2010 to 2020) was descending (e.g., see the blue colors in Fig. 7(c)). During the second decade (Fig. 7(d)), 52 % of the drought trend map experienced a TVMDI decline ranging from 0 to -0.01. However, less than 32% of the area indicated varying ranges of dispersed drought prevalence across the country.

Over the twenty-year period initiated from 2000, drought severity has undergone noticeable alterations (Fig. 7(e)). While the overall trend of drought severity significantly alleviated, there were still sparse regions suffering from drought growth. The areas with intense drought deterioration were mostly observed in the central, northern, western and south-westernmost areas which account for almost 11% of the total area. Overall, the central regions along with the northern coastal parts have been dealing with the slight-ascending drought conversions which account for approximately a 16% of the entire study area.

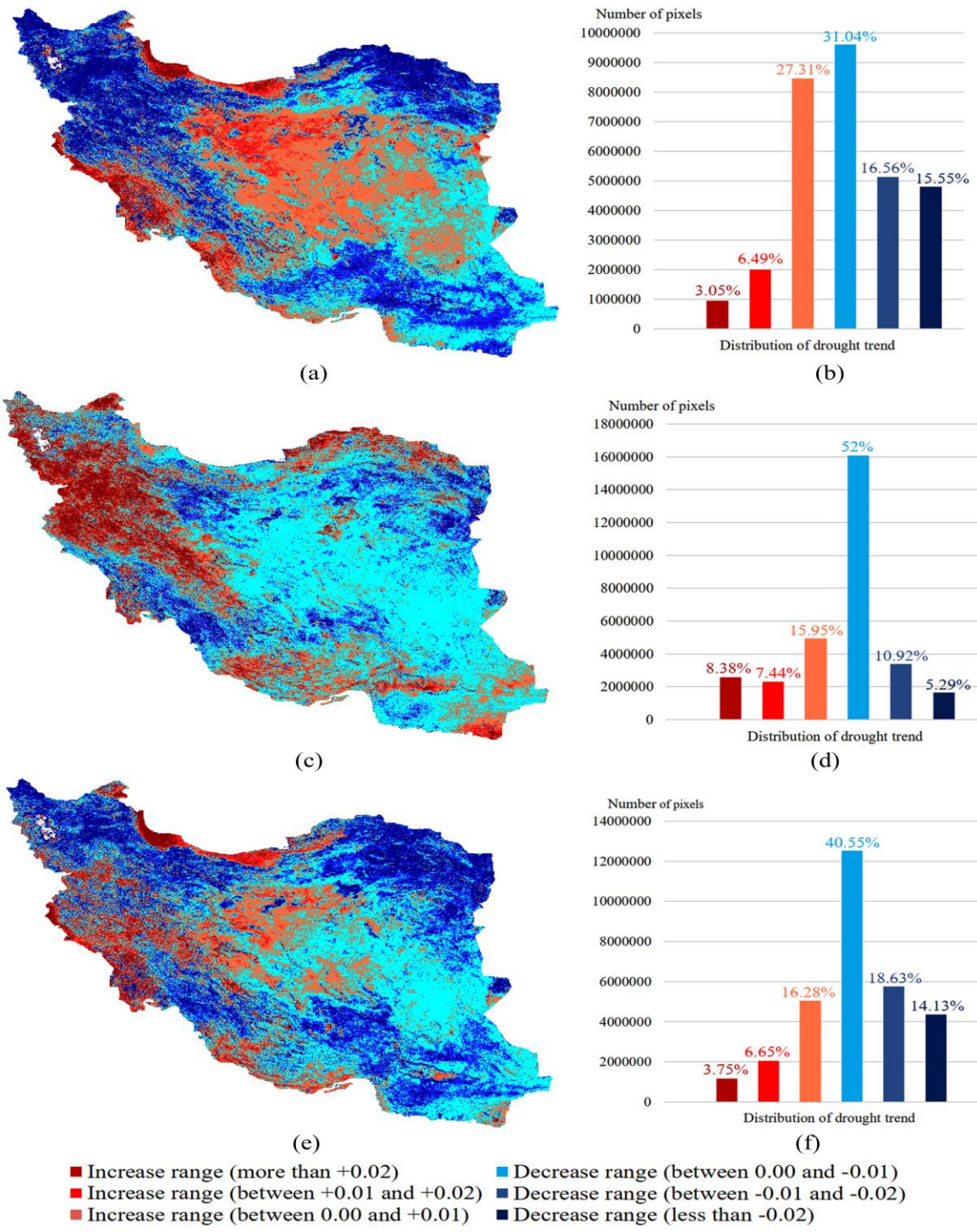

Figure 7. Spatial distribution of drought trend maps between (a) 2000 and 2010 (c) 2010 and 2020 (e) 2000 and 2020. (b), (d) and (f) are the bar charts for distribution of drought trends that correspond to the maps illustrated in (a), (c) and (e), respectively.

4.2.3 Classification maps of drought severity

The spatial drought risk maps of Iran corresponding to the years 2000, 2005, 2010, 2015 and 2020 are respectively demonstrated in Fig. 8. The classification ranges of TVMPDI used in Fig. 8 are also presented provided in Table 4. The classification ranges were set in a way that the spatial drought risk maps were consistent with our knowledge from the study area. In fact, the wettest region in Iran can be found alongside the Caspian Sea in the north, while the extensively dry areas are related to the Lut and Kavir deserts.

Table 4. Classification of TVMPDI drought index used in Fig. 8.

Drought class	TVMPDI range	Drought class	TVMPDI range
Extremely arid	[0.75,1]	Wet	[0.35,0.45]
Moderately arid	[0.65,0.75]	Moderate wet	[0.25,0.35]
Arid	[0.55,0.65]	Extremely wet	[0,0.25]
Natural	[0.45,0.55]		

In accordance with previous results, Fig. 8 also emphasizes that the year 2000 had the most intense drought. This can be seen by considering the extremely arid regions (red class) that are scattered across the southeast in 2000 more extensively. The extent of these regions reduced over the next 20 years (see the drought classified maps in 2005, 2010, 2015 and 2020). The outstanding point is that the natural and wet classes considerably increased over the 20-year period as the regions in cyan and purple expanded in the maps ululated in Fig. 8. For instance, starting from 3.04% in 2000, the wet class of drought covered 4.44%, 6.68%, 5.37%, and 5.33% of the entire country area in 2005, 2010, 2015, and 2020 respectively.

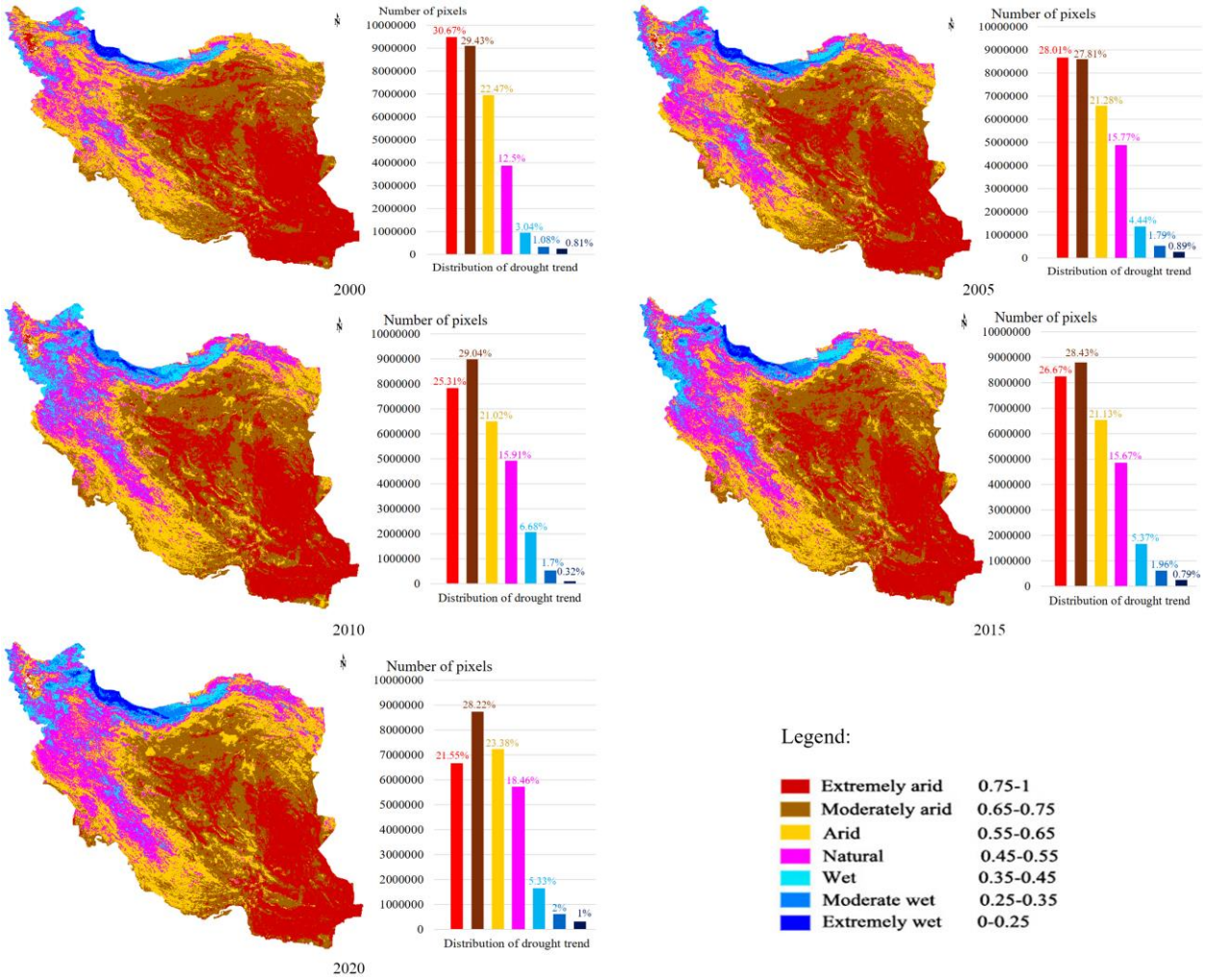

Figure 8. The spatial drought risk map across Iran for the years 2000, 2005, 2010, 2015, and 2020.

4.2.4 Local drought monitoring within the provinces of Iran

Although the overall drought trend across Iran gradually decreased with multiple oscillations over the past 21 years (shown in Fig. 6, 7 and 8), drought trends within each province of Iran have been monitored to specify drought risk level in local scales. To this end, the drought changes of all 31 provinces of Iran were monitored using the TVMPDI index and the results were extracted (and shown in Fig. 10 in the Appendix section). The TVMPDI values in the graphs of Fig. 10 were

averaged for every 6 months over the 20-year period starting from 20th March 2000. These results were obtained from the 6-month dryness maps of provinces for the aforementioned period.

Using such graphs, the average dryness of each province during the 21 years was extracted that indicates the level of overall dryness in each province (Fig. 9(a)). To have an overview of the overall trends within the provinces during the 21 years, the best fit trendlines were recorded. The slope of the trendlines in the provinces which represented the general direction and intensity of the drought fluctuations was also extracted and shown in Fig. 9(b). Such spatio-temporal drought trend analysis using RS data can be considered as the main privilege against site-based drought analysis that is usually done by station-based meteorological data.

The overall dryness of provinces of Iran during the 21 years was mapped and shown in Fig. 9(a), where the darker brown colors specify the drier provinces. Considering Fig. 9(a), the provinces located in the eastern half of Iran showed the highest drought values.

The drought trend map of the provinces of Iran shows that the provinces located in the central regions from the north to the south are mostly affected by risky drought trends. Among all provinces, Isfahan and Gilan were the only provinces showing the positive slope of the drought trendline (Fig. 9(b)). The largest descending slopes of the drought trendline were related to West Azerbaijan, East Azerbaijan, Hormozgan, Qazvin, Zanjan, and Ilam which are mostly located in the west half of the country. Accordingly, the provinces excluding the aforementioned cases demonstrated a mild declining trend.

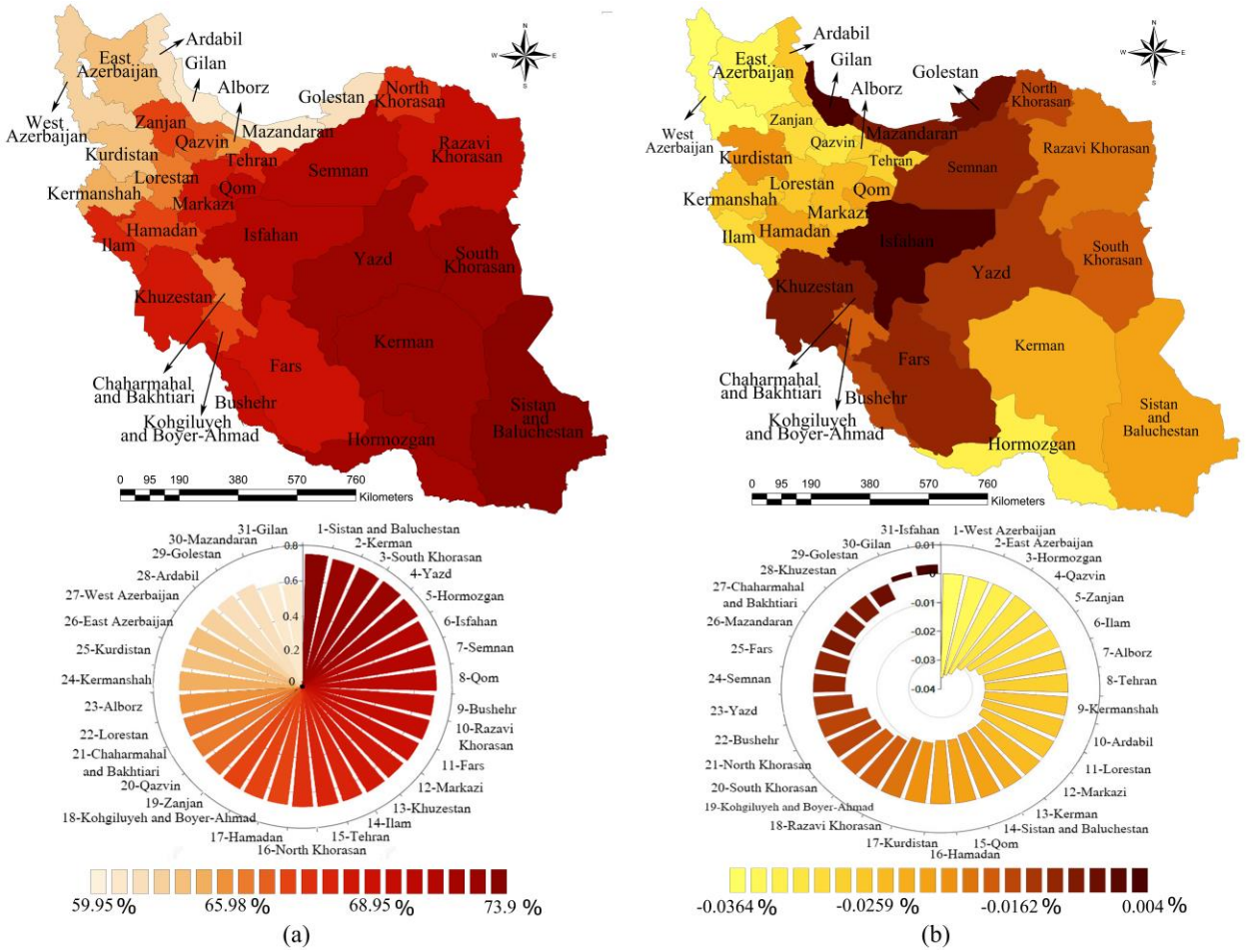

Figure 9. (a) TVMPDI dryness map and ranking of the provinces of Iran over 2000-2020 period (b) TVMPDI drought trend map of provinces of Iran (d) Drought trend map and ranking of the provinces of Iran using the TVMPDI oscillations.

5. Discussion

The reason why the TVMPDI could outperform the other indices is probably due to the precipitation data and SM that are involved in this index. Among the four drought indicators used in this index, SM and TRMM/GPM precipitation are inherently close to the nature of *in-situ* precipitation data. According to Table 3, the TRMM/GPM precipitation data used in TVMPDI was correlated with *in-situ* data at 0.93 *r* value.

It should be noted that the provision of various environmental data like SM, LST, vegetation and precipitation for large-scale and long-term drought monitoring studies using meteorological data is extremely costly, time-consuming, and very challenging. The status of some data like vegetation can not truly be measured by station-based methods as well. The meteorological-station-based methods that employ different models to turn the station-based maps into fine resolution drought maps inevitably incorporate inaccurate estimates in modeled areas. This is because the variation of environmental and climatic changes can be highly inconsistent in regions having no measuring station. Similar to the drought map results in (Orimoloye et al., 2019), the trend maps of drought in this study were built using the classification of difference maps in fig. 7 to show any inconsistency of drought changes.

The *in-situ* precipitation data showed that Iran experienced unprecedented rainfall and the highest mean cumulative annual precipitation in 2019 over the past 21 years. However, the drought map of the 2020 period showed that drought increased in several regions compared to the drought map of the 2000 period (see Fig. 7(e)). According to (Orimoloye et al., 2021b), Iran was reported to have no risk of drought disaster impact on agriculture in 2020. This is consistent with the results of this study shown in fig. 5, 6 and 7. Similar to the drought severity maps in (Du et al., 2019) used for spatio-temporal drought analyses, the drought severity maps of this (fig. 8) study revealed the frequency of drought incidence over 21 years.

As the classification of drought intensity has been known as a valuable method for drought severity analyses (Junqueira et al., 2020), fig. 8 of this paper revealed that Isfahan province can be regarded as a high-risk region in terms of drought side-effects in future. The ranking of the provinces dryness shown in Fig. 9(a) states that Gilan, Mazandaran and Golestan were the wettest provinces during the whole 20-year period respectively. Conversely, Sistan and Baluchestan,

Kerman and South Khorasan were the driest provinces respectively. In general, Isfahan and Gilan can be considered as endangered provinces in terms of environmental sustainability challenges because their TVMPDI trendline slopes are positive (Fig. 9(b)). This is consistent with the results of Eslamian and Jahadi, (2019) where drought monitoring in Isfahan stations is reported to have indicated a considerable reduction of wet magnitude based on both SPI and SPEI indices. Considering fig. 7 and 8, Khuzestan province also faced drought prevalence that has frequently been occurred in several years. This is consistent with the results reported by (Sobhani et al., 2020; Sobhani and Zengir, 2020). The descending slopes of the drought trendline in West Azerbaijan, East Azerbaijan that were shown in fig. 9(b) are consistent with the results reported by SafarianZengir et al., (2020).

6. Conclusion

In this study, the TVMPDI RSDI was proposed and validated. It was found that TVMPDI had the highest *r* with the *in-situ* precipitation and SPI results. The SM and precipitation drought indicators involved in TVMPDI were probably the main reason for its high accuracy. The results of drought monitoring showed that Iran experienced the most severe drought in 2000, while the least level of drought intensity was observed in 2019. Overall changes in drought indicated a descending trend over the past two decades using all RSDIs. However, drought monitoring at the province level revealed a drought exacerbation in Isfahan, Gilan and Khuzestan showing incremental drought levels. Considering both province- and country-wide drought trends for the past two decades, Isfahan was recognized as the most endangered province. The spatio-temporal analysis of this study showed that severe drought effects can occur in central Iran. This is due to the worrying slopes of the drought trendlines of these local regions that are close to be positive. The seasonal analysis of drought trend using different RSDIs also showed that Winter was the only

season having an ascending slope, and the most descending drought trend was found in the Spring season. Due to the far-reaching effects of drought on human life, the results of this study can help the officials for better management in different fields such as agriculture, water supply, urban development, natural resources and economy.

The limitation of this study is probably the 20-year period of monitoring that could have been much longer if other RS satellites (i.e., Landsat series) had been employed. Using the results of RS systems integrated with meteorological data for quantitatively/qualitatively characterizing different types of drought is presumably the most cost-effective and accurate solution addressing the drought monitoring concerns. Analyzing the sequential trend maps (i.e., year by year maps) of drought in future studies can arguably result in having precious information on spatial patterns of drought expansion that occurred over time.

Acknowledgement

We appreciate the I.R. of Iran Meteorological Organization (IRIMO) that provided us with meteorological data.

Appendix

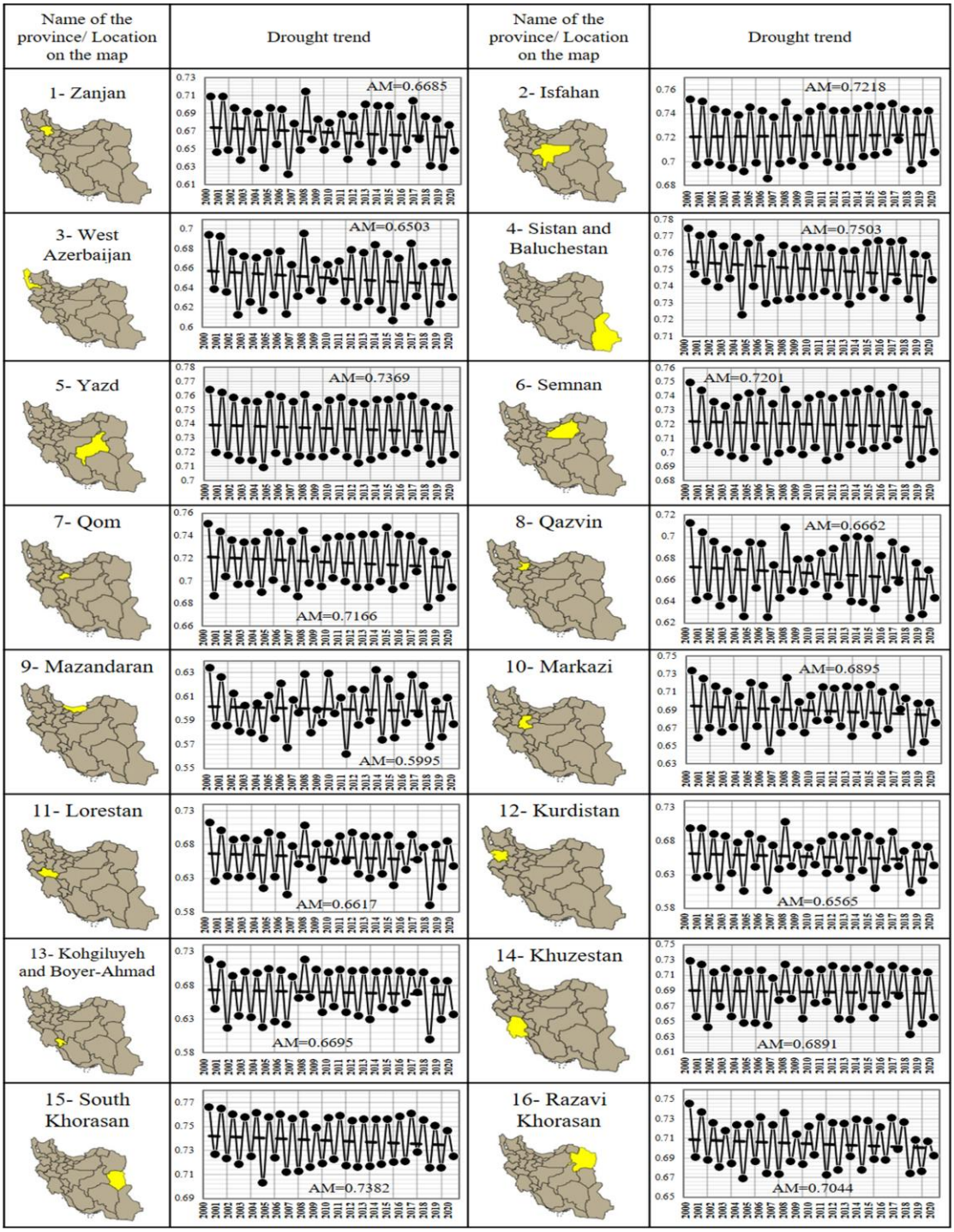

Figure 10. (continued).

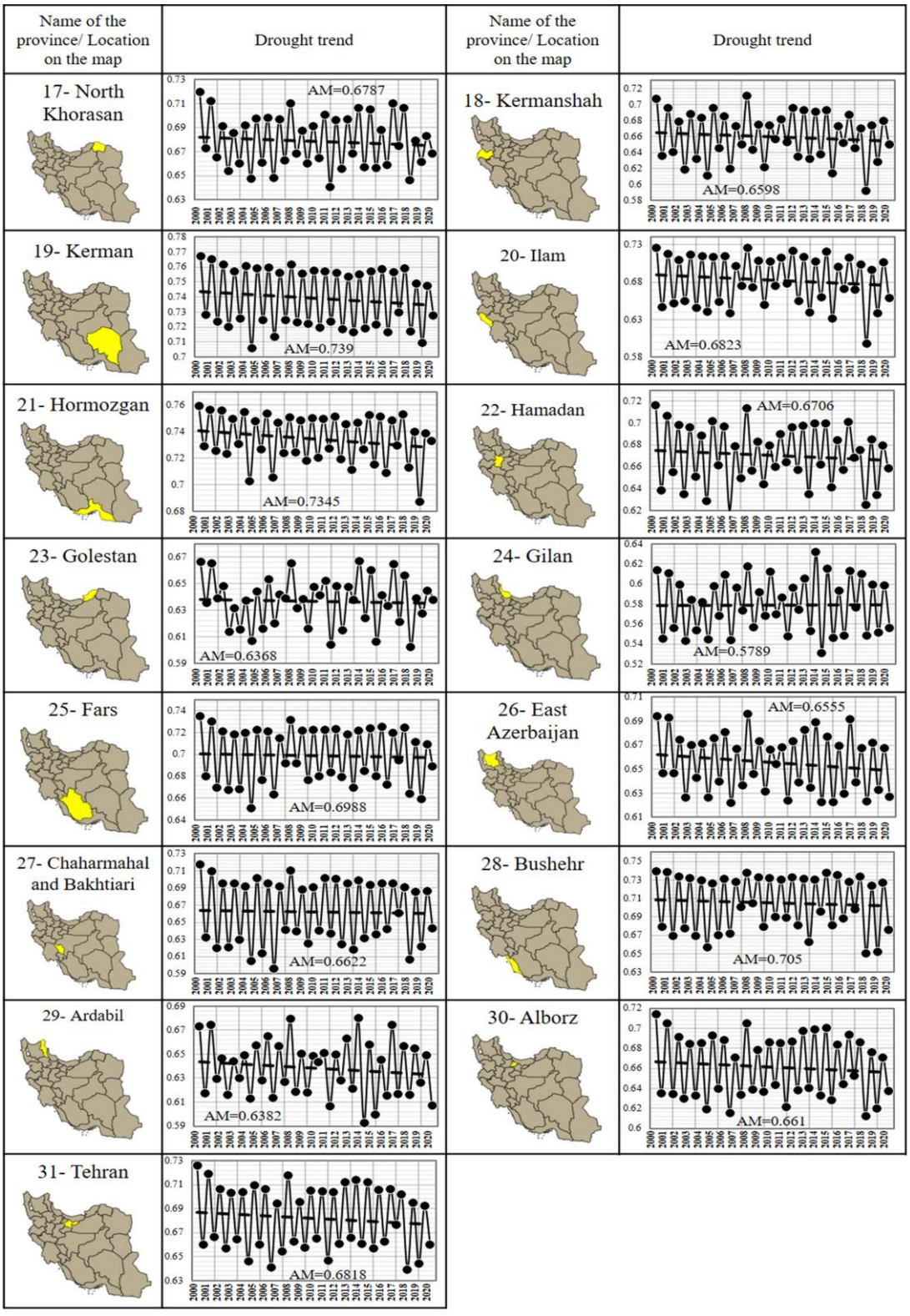

Figure 10. Drought trend using 6-month TVMPDI values for each province of Iran during 2000-2020. AM stands for Average Mean that is the average level of drought over 20 years.

References

Adedeji, O., Olusola, A., James, G., Shaba, H.A., Orimoloye, I.R., Singh, S.K., Adelabu, S., 2020. Early warning systems development for agricultural drought assessment in Nigeria. Environ. Monit. Assess. 192, 1–21.

AghaKouchak, A., Farahmand, A., Melton, F.S., Teixeira, J., Anderson, M.C., Wardlow, B.D., Hain, C.R., 2015. Remote sensing of drought: Progress, challenges and opportunities. Rev. Geophys. 53, 452–480.

Aksoy, S., Gorucu, O., Sertel, E., 2019. Drought Monitoring using MODIS derived indices and Google Earth Engine Platform, in: 2019 8th International Conference on Agro-Geoinformatics (Agro-Geoinformatics). pp. 1–6.

Alizadeh-Choobari, O., Najafi, M.S., 2018. Extreme weather events in Iran under a changing climate. Clim. Dyn. 50, 249–260.

Amani, M., Ghorbanian, A., Ahmadi, S.A., Kakooei, M., Moghimi, A., Mirmazloumi, S.M., Moghaddam, S.H.A., Mahdavi, S., Ghahremanloo, M., Parsian, S., Wu, Q., Brisco, B., 2020a. Google Earth Engine Cloud Computing Platform for Remote Sensing Big Data Applications: A Comprehensive Review. IEEE J. Sel. Top. Appl. Earth Obs. Remote Sens. 13, 5326–5350. https://doi.org/10.1109/JSTARS.2020.3021052

Amani, M., Kakooei, M., Moghimi, A., Ghorbanian, A., Ranjgar, B., Mahdavi, S., Davidson, A., Fisette, T., Rollin, P., Brisco, B., Others, 2020b. Application of Google Earth Engine Cloud Computing Platform, Sentinel Imagery, and Neural Networks for Crop Mapping in Canada. Remote Sens. 12, 3561.

Amani, M., Parsian, S., MirMazloumi, S.M., Aieneh, O., 2016. Two new soil moisture indices based on the NIR-red triangle space of Landsat-8 data. Int. J. Appl. Earth Obs. Geoinf. 50, 176–186.

Amani, M., Salehi, B., Mahdavi, S., Masjedi, A., Dehnavi, S., 2017. Temperature-vegetation-soil moisture dryness index (TVMDI). Remote Sens. Environ. 197, 1–14.

Amirataee, B., Montaseri, M., 2017. The performance of SPI and PNPI in analyzing the spatial and temporal trend of dry and wet periods over Iran. Nat. Hazards 86, 89–106.

Anderson, M.C., Zolin, C.A., Hain, C.R., Semmens, K., Yilmaz, M.T., Gao, F., 2015. Comparison of satellite-derived LAI and precipitation anomalies over Brazil with a thermal infrared-based Evaporative Stress Index for 2003–2013. J. Hydrol. 526, 287–302.

Bajgiran, P.R., Darvishsefat, A.A., Khalili, A., Makhdoum, M.F., 2008. Using AVHRR-based vegetation indices for drought monitoring in the Northwest of Iran. J. Arid Environ. 72, 1086–1096.

Byun, H.-R., Wilhite, D.A., 1999. Objective quantification of drought severity and duration. J. Clim. 12, 2747–2756.

Córdova, O., Venturini, V., Walker, E., 2020. Drought monitoring in El Salvador through remotely sensed variables using the Google Earth Engine platform. Rev. Teledetección 93–103.

Darand, M., Daneshvar, M.R.M., 2014. Regionalization of precipitation regimes in Iran using principal component analysis and hierarchical clustering analysis. Environ. Process. 1, 517–532.

Ding, S., Rulinda, C.M., Stein, A., Bijker, W., 2011. NDVI time series and Markov chains to model the change of fuzzy vegetative drought classes. 2011 6th Int. Work. Anal. Multi-Temporal Remote Sens. Images, Multi-Temp 2011 - Proc. 201–204. https://doi.org/10.1109/Multi-Temp.2011.6005083

Du, J., Kimball, J.S., Velicogna, I., Zhao, M., Jones, L.A., Watts, J.D., Kim, Y., 2019. Multicomponent satellite assessment of drought severity in the contiguous United States from 2002 to 2017 using AMSR-E and AMSR2. Water Resour. Res. 55, 5394–5412.

Du, L., Tian, Q., Yu, T., Meng, Q., Jancso, T., Udvardy, P., Huang, Y., 2013. A comprehensive drought monitoring method integrating MODIS and TRMM data. Int. J. Appl. Earth Obs. Geoinf. 23, 245–253.

Dyosi, M., Kalumba, A.M., Magagula, H.B., Zhou, L., Orimoloye, I.R., 2021. Drought conditions appraisal using geoinformatics and multi-influencing factors. Environ. Monit. Assess. 193, 1–19.

Ebrahimy, H., Aghighi, H., Azadbakht, M., Amani, M., Mahdavi, S., Matkan, A.A., 2021. Downscaling MODIS Land Surface Temperature Product Using an Adaptive Random Forest Regression Method and Google Earth Engine for a 19-Years Spatiotemporal Trend Analysis Over Iran. IEEE J. Sel. Top. Appl. Earth Obs. Remote Sens. 14, 2103–2112.

Emadodin, I., Reinsch, T., Taube, F., 2019. Drought and desertification in Iran. Hydrology 6, 66.

Eslamian, S., Jahadi, M., 2019. Monitoring and prediction of drought by Markov chain model based on SPI and new index in Isfahan. Int. J. Hydrol. Sci. Technol. 9, 355–365.

Farahmand, A., AghaKouchak, A., 2015. A generalized framework for deriving nonparametric standardized drought indicators. Adv. Water Resour. 76, 140–145.

Gao, B.-C., 1996. NDWI—A normalized difference water index for remote sensing of vegetation liquid water from space. Remote Sens. Environ. 58, 257–266.

Ghaleb, F., Mario, M., Sandra, A.N., 2015. Regional landsat-based drought monitoring from 1982 to 2014. Climate 3, 563–577.

Ghorbanian, A., Kakooei, M., Amani, M., Mahdavi, S., Mohammadzadeh, A., Hasanlou, M., 2020. Improved land cover map of Iran using Sentinel imagery within Google Earth Engine and a novel automatic workflow for land cover classification using migrated training samples. ISPRS J. Photogramm. Remote Sens. 167, 276–288. https://doi.org/10.1016/J.ISPRSJPRS.2020.07.013

Ghulam, A., Qin, Q., Teyip, T., Li, Z.-L., 2007. Modified perpendicular drought index (MPDI): a real-time drought monitoring method. ISPRS J. Photogramm. Remote Sens. 62, 150–164.

Gorelick, N., Hancher, M., Dixon, M., Ilyushchenko, S., Thau, D., Moore, R., 2017. Google Earth Engine: Planetary-scale geospatial analysis for everyone. Remote Sens. Environ. 202, 18–27. https://doi.org/10.1016/j.rse.2017.06.031

Guo, H., Bao, A., Liu, T., Ndayisaba, F., Jiang, L., Zheng, G., Chen, T., De Maeyer, P., 2019. Determining variable weights for an optimal scaled drought condition index (OSDCI): Evaluation in central Asia. Remote Sens. Environ. 231, 111220.

Han, Y., Li, Z., Huang, C., Zhou, Y., Zong, S., Hao, T., Niu, H., Yao, H., 2020. Monitoring droughts in the Greater Changbai Mountains using multiple remote sensing-based drought indices. Remote Sens. 12, 530.

Hao, C., Zhang, J., Yao, F., 2015. Combination of multi-sensor remote sensing data for drought monitoring over Southwest China. Int. J. Appl. Earth Obs. Geoinf. 35, 270–283.

Hao, Z., AghaKouchak, A., 2014. A nonparametric multivariate multi-index drought monitoring framework. J. Hydrometeorol. 15, 89–101.

Hao, Z., Yuan, X., Xia, Y., Hao, F., Singh, V.P., 2017. An overview of drought monitoring and prediction systems at regional and global scales. Bull. Am. Meteorol. Soc. 98, 1879–1896.

Heydari, H., Valadan Zoej, M., Maghsoudi, Y., Dehnavi, S., 2018. An investigation of drought prediction using various remote-sensing vegetation indices for different time spans. Int. J. Remote Sens. 39, 1871–1889.

Hosseini, A., Ghavidel, Y., Khorshiddoust, A.M., Farajzadeh, M., 2020. Spatio-temporal analysis of dry and

wet periods in Iran by using Global Precipitation Climatology Center-Drought Index (GPCC-DI). Theor. Appl. Climatol. 1–11.

Huang, J., Zhuo, W., Li, Y., Huang, R., Sedano, F., Su, W., Dong, J., Tian, L., Huang, Y., Zhu, D., 2020. Comparison of three remotely sensed drought indices for assessing the impact of drought on winter wheat yield. Int. J. Digit. Earth 13, 504–526.

Huffman, G.J., Bolvin, D.T., Nelkin, E.J., Wolff, D.B., Adler, R.F., Gu, G., Hong, Y., Bowman, K.P., Stocker, E.F., 2007. The TRMM Multisatellite Precipitation Analysis (TMPA): Quasi-global, multiyear, combined-sensor precipitation estimates at fine scales. J. Hydrometeorol. 8, 38–55.

Junqueira, R., Viola, M.R., de Mello, C.R., Vieira-Filho, M., Alves, M.V.G., Amorim, J. da S., 2020. Drought severity indexes for the Tocantins River Basin, Brazil. Theor. Appl. Climatol. 141, 465–481.

Khan, R., Gilani, H., Iqbal, N., Shahid, I., 2020. Satellite-based (2000--2015) drought hazard assessment with indices, mapping, and monitoring of Potohar plateau, Punjab, Pakistan. Environ. Earth Sci. 79, 23.

Kogan, F.N., 1995. Droughts of the late 1980s in the United States as derived from NOAA polar-orbiting satellite data. Bull. - Am. Meteorol. Soc. https://doi.org/10.1175/1520-0477(1995)076<0655:DOTLIT>2.0.CO;2

Labarrere, C.A., Woods, J.R., Hardin, J.W., Campana, G.L., Ortiz, M.A., Jaeger, B.R., Reichart, B., Bonnin, J.M., Currin, A., Cosgrove, S., 2011. Early prediction of cardiac allograft vasculopathy and heart transplant failure. Am. J. Transplant. 11, 528–535.

Liu, X., Zhu, X., Pan, Y., Li, S., Liu, Y., Ma, Y., 2016. Agricultural drought monitoring: Progress, challenges, and prospects. J. Geogr. Sci. 26, 750–767.

Mahmoudi, P., Rigi, A., Kamak, M.M., 2019. A comparative study of precipitation-based drought indices with the aim of selecting the best index for drought monitoring in Iran. Theor. Appl. Climatol. 137, 3123–3138.

McKee, T.B., Doesken, N.J., Kleist, J., 1993. The relationship of drought frequency and duration to time scales, in: Proceedings of the 8th Conference on Applied Climatology. Boston, pp. 179–183.

Oesting, M., Stein, A., 2018. Spatial modeling of drought events using max-stable processes. Stoch. Environ. Res. Risk Assess. 32, 63–81. https://doi.org/10.1007/s00477-017-1406-z

Okal, H., Ngetich, F., Okeyo, J., 2020. Spatio-temporal characterisation of droughts using selected indices in Upper Tana River Watershed, Kenya. Sci. African e00275.

Orimoloye, I.R., Belle, J.A., Ololade, O.O., 2021a. Drought disaster monitoring using MODIS derived index for drought years: A space-based information for ecosystems and environmental conservation. J. Environ. Manage. 284, 112028.

Orimoloye, I.R., Belle, J.A., Olusola, A.O., Busayo, E.T., Ololade, O.O., 2021b. Spatial assessment of drought disasters, vulnerability, severity and water shortages: a potential drought disaster mitigation strategy. Nat. Hazards 105, 2735–2754.

Orimoloye, I.R., Ololade, O.O., Belle, J.A., 2021c. Satellite-based application in drought disaster assessment using terra MOD13Q1 data across free state province, South Africa. J. Environ. Manage. 285, 112112.

Orimoloye, I.R., Ololade, O.O., Mazinyo, S.P., Kalumba, A.M., Ekundayo, O.Y., Busayo, E.T., Akinsanola, A.A., Nel, W., 2019. Spatial assessment of drought severity in Cape Town area, South Africa. Heliyon 5, e02148.

Raziei, T., Bordi, I., Pereira, L.S., 2013. Regional drought modes in Iran using the SPI: the effect of time scale and spatial resolution. Water Resour. Manag. 27, 1661–1674.

Raziei, T., Bordi, I., Pereira, L.S., 2011. An application of GPCC and NCEP/NCAR datasets for drought variability analysis in Iran. Water Resour. Manag. 25, 1075–1086.

Rulinda, C.M., Bijker, W., Stein, A., 2010. Image mining for drought monitoring in eastern Africa using Meteosat SEVIRI data. Int. J. Appl. Earth Obs. Geoinf. 12. https://doi.org/10.1016/j.jag.2009.10.008

Rulinda, C.M., Bijker, W., Steina, A., 2011. The chlorophyll variability in Meteosat derived NDVI in a context of drought monitoring. Procedia Environ. Sci. 3, 32–37. https://doi.org/10.1016/j.proenv.2011.02.007

Rulinda, C.M., Dilo, A., Bijker, W., Stein, A., 2012. Characterising and quantifying vegetative drought in East Africa using fuzzy modelling and NDVI data. J. Arid Environ. 78, 169–178. https://doi.org/10.1016/j.jaridenv.2011.11.016

Rulinda, C.M., Stein, A., Turdukulov, U.D., 2013. Visualizing and quantifying the movement of vegetative drought using remote-sensing data and GIS. Int. J. Geogr. Inf. Sci. 27, 1481–1496. https://doi.org/10.1080/13658816.2012.723712

SafarianZengir, V., Sobhani, B., Asghari, S., 2020. Modeling and monitoring of drought for forecasting it, to reduce natural hazards atmosphere in western and north western part of Iran, Iran. Air Qual. Atmos. Heal. 13, 119–130.

Sandholt, I., Rasmussen, K., Andersen, J., 2002. A simple interpretation of the surface temperature/vegetation index space for assessment of surface moisture status. Remote Sens. Environ. 79, 213–224.

Sanei, A., Zakaria, M., 2011. Distribution pattern of the Persian leopard (Panthera pardus saxicolor) in Iran. Asia Life Sci. Suppl. 7, 7–18.

Sazib, N., Mladenova, I., Bolten, J., 2018. Leveraging the google earth engine for drought assessment using global soil moisture data. Remote Sens. 10, 1265.

Schirmbeck, L.W., Fontana, D.C., Schirmbeck, J., 2018. Two approaches to calculate TVDI in humid subtropical climate of southern Brazil. Sci. Agric. 75, 111–120.

ShadA, M.S., IldoromiB, A., AkhzariC, D., 2017. Drought Monitoring Using Vegetation Indices and MODIS Data (Case Study: Isfahan Province, Iran). J. Rangel. Sci. 7, 148.

Shahabfar, A., Ghulam, A., Eitzinger, J., 2012. Drought monitoring in Iran using the perpendicular drought indices. Int. J. Appl. Earth Obs. Geoinf. 18, 119–127.

Sharafati, A., Nabaei, S., Shahid, S., 2020. Spatial assessment of meteorological drought features over different climate regions in Iran. Int. J. Climatol. 40, 1864–1884.

Skofronick-Jackson, G., Petersen, W.A., Berg, W., Kidd, C., Stocker, E.F., Kirschbaum, D.B., Kakar, R., Braun, S.A., Huffman, G.J., Iguchi, T., 2017. The Global Precipitation Measurement (GPM) mission for science and society. Bull. Am. Meteorol. Soc. 98, 1679–1695.

Sobhani, B., Zengir, V.S., 2020. Modeling, monitoring and forecasting of drought in south and southwestern Iran, Iran. Model. Earth Syst. Environ. 6, 63–71.

Sobhani, B., Zengir, V.S., Kianian, M.K., 2019. Drought monitoring in the Lake Urmia basin in Iran. Arab. J. Geosci. 12, 1–15.

Sobhani, B., Zengir, V.S., Yazdani, M.H., 2020. Modelling, evaluation and simulation of drought in Iran, southwest Asia. J. Earth Syst. Sci. 129, 1–13.

Wang, F., Wang, Z., Yang, H., Zhao, Y., Li, Z., Wu, J., 2018. Capability of remotely sensed drought indices for representing the spatio–temporal variations of the meteorological droughts in the Yellow River Basin. Remote Sens. 10, 1834.

Wang, H., Lin, H., Liu, D., 2014. Remotely sensed drought index and its responses to meteorological drought in Southwest China. Remote Sens. Lett. 5, 413–422.

West, H., Quinn, N., Horswell, M., 2019. Remote sensing for drought monitoring & impact assessment: Progress, past challenges and future opportunities. Remote Sens. Environ. 232, 111291.

Xu, L., Abbaszadeh, P., Moradkhani, H., Chen, N., Zhang, X., 2020. Continental drought monitoring using satellite soil moisture, data assimilation and an integrated drought index. Remote Sens. Environ. 250, 112028.

Zambrano, F., Lillo-Saavedra, M., Verbist, K., Lagos, O., 2016. Sixteen years of agricultural drought assessment of the BioBío region in Chile using a 250 m resolution Vegetation Condition Index (VCI). Remote Sens. 8, 530.

Zambrano, F., Wardlow, B., Tadesse, T., Lillo-Saavedra, M., Lagos, O., 2017. Evaluating satellite-derived long-term historical precipitation datasets for drought monitoring in Chile. Atmos. Res. 186, 26–42.

Zarch, M.A.A., Malekinezhad, H., Mobin, M.H., Dastorani, M.T., Kousari, M.R., 2011. Drought monitoring by reconnaissance drought index (RDI) in Iran. Water Resour. Manag. 25, 3485–3504.

Zarei, R., Sarajian, M., Bazgeer, S., 2013. Monitoring meteorological drought in Iran using remote sensing and drought indices. Desert 18, 89–97.

Zhang, A., Jia, G., 2013. Monitoring meteorological drought in semiarid regions using multi-sensor microwave remote sensing data. Remote Sens. Environ. 134, 12–23.

Zhang, J., Mu, Q., Huang, J., 2016. Assessing the remotely sensed Drought Severity Index for agricultural drought monitoring and impact analysis in North China. Ecol. Indic. 63, 296–309.

Zhou, X., Wang, P., Tansey, K., Zhang, S., Li, H., Wang, L., 2020. Developing a fused vegetation temperature condition index for drought monitoring at field scales using Sentinel-2 and MODIS imagery. Comput. Electron. Agric. 168, 105144.

Zormand, S., Jafari, R., Koupaei, S.S., 2017. Assessment of PDI, MPDI and TVDI drought indices derived from MODIS Aqua/Terra Level 1B data in natural lands. Nat. Hazards 86, 757–777.